P2.53

LABORATORY EXPERIMENTS OF ICE FORMATION IN CLOUD SIMULATION CHAMBER

Takuya Tajiri *, Masataka Murakami, Narihiro Orikasa, Atsushi Saito, and Kenichi Kusunoki
Meteorological Research Institute, Tsukuba, Japan

1. INTRODUCTION

Ice is essential for precipitation associated with many mid-latitude clouds that have extensive supercooled regions, lending themselves to copious ice production. Besides the effect of ice on cloud microphysical and radiative properties, especially for upper-level clouds, ice has a notable impact on large scale climate because significant changes in cloud optical depth and cloud fraction result from altering the partitioning between cloud ice and supercooled cloud water. In order to improve quantitative precipitation forecasts and to predict climate changes, therefore, the initial formation of ice is one of the most important processes.

Phase change into ice (ice nucleation) takes place increasingly by homogeneous freezing of pure water and solution droplets below about -35°C, or is heterogeneously induced by ice forming nuclei (IN) which exhibit four basic modes of action (e.g., Pruppacher and Klett, 1997). However, it is not sufficiently understood how ice crystals form in clouds under different atmospheric conditions. The crucial questions regarding the behavior of aerosol particles in natural ice initiation processes remain.

To investigate the details of the fundamental processes of cloud formation, a new cloud simulation chamber was built in 2005 at Meteorological Research Institute (MRI), Japan Meteorological Agency. The MRI chamber was designed for controlled-expansion type chamber (DeMott and Rogers 1990), so that both temperature and pressure in experimental volume are automatically controlled to simulate the natural processes (adiabatic expansion). Also, It is a great advantage that initial conditions and thermodynamic histories are well-defined. The MRI chamber was started up for studies of ice formation and has been utilized in an attempt to identify ice nucleation modes and to quantify ice crystal concentrations activated under various tropospheric cloud conditions. This paper describes an overview of basic features and instrumentation of MRI chamber and preliminary results in a first set of experiments.

* *Corresponding author address:* Takuya Tajiri, Meteorological Research Institute, 1-1, Nagamine, Tsukuba, Ibaraki 305-0052, Japan; e-mail: ttajiri@mri-jma.go.jp

2. BASIC FEATURES OF MRI CHAMBER

Figures 1 and 2 show a schematic diagram and photograph of the MRI cloud simulation chamber with technical components and instrumentation. The chamber consists of two stainless vessels, that is, the outer pressure-controlled chamber and the inner temperature-controlled chamber. Inner cylindrical vessel (i.e., experimental working volume) has a height of 1.8m, a diameter of 1 m, and thus a volume of 1.4m^3. The outer chamber has a variety of ports to accommodate a versatile experiment. The chamber pressure can be decreased down to below 30hPa and its evacuation rate are adjustable by using a vacuum pump, pressure-driven bypass control valve and switching valves in different sizes connected to the outer chamber. Two Pressure transducers (PTB210, VAISALA) measure inner/outer chamber pressure. The inner vessel can be cooled to any temperature between 30 to -100°C by circulating the coolant, unfreeze fluid (NOVEC HFE-7100). Four large refrigerators (4000PXA-X, MAC) are used to cool the fluid and consequently to decrease the reservoir temperature. The fluid running paths inside the chamber interior surface are subdivided into thirteen panels (wall) and two plate coils (top and bottom), in order to realize mean air temperature homogeneity. 8 thermocouples measure the air temperature T_a several cm into the inner volume and 23 thermocouples measure the chamber interior surface temperature T_w, located at different levels. The air temperature inhomogeneity amounts less than ±0.3 °C under static condition.

Sample air including generated aerosol particles or natural outdoor air can be introduced into the inner chamber prior to an adiabatic expansion. The particle injection (air supply) port is located at the top of the chamber. A small fan stirs the injected air to achieve homogeneity inside the volume. Chamber humidity is decreased by the addition of dry air until it just approaches to a desired dewpoint, for sample air dewpoint temperature T_{dew} is usually higher than desired value. T_{dew} is measured by two chilled mirror hygrometers (MODEL300 and 137, EdgeTech) and used with T_a to calculate the humidity.

3. ADIABATIC ASCENT CONTROLL

The introduction rate of coolant to the circulating

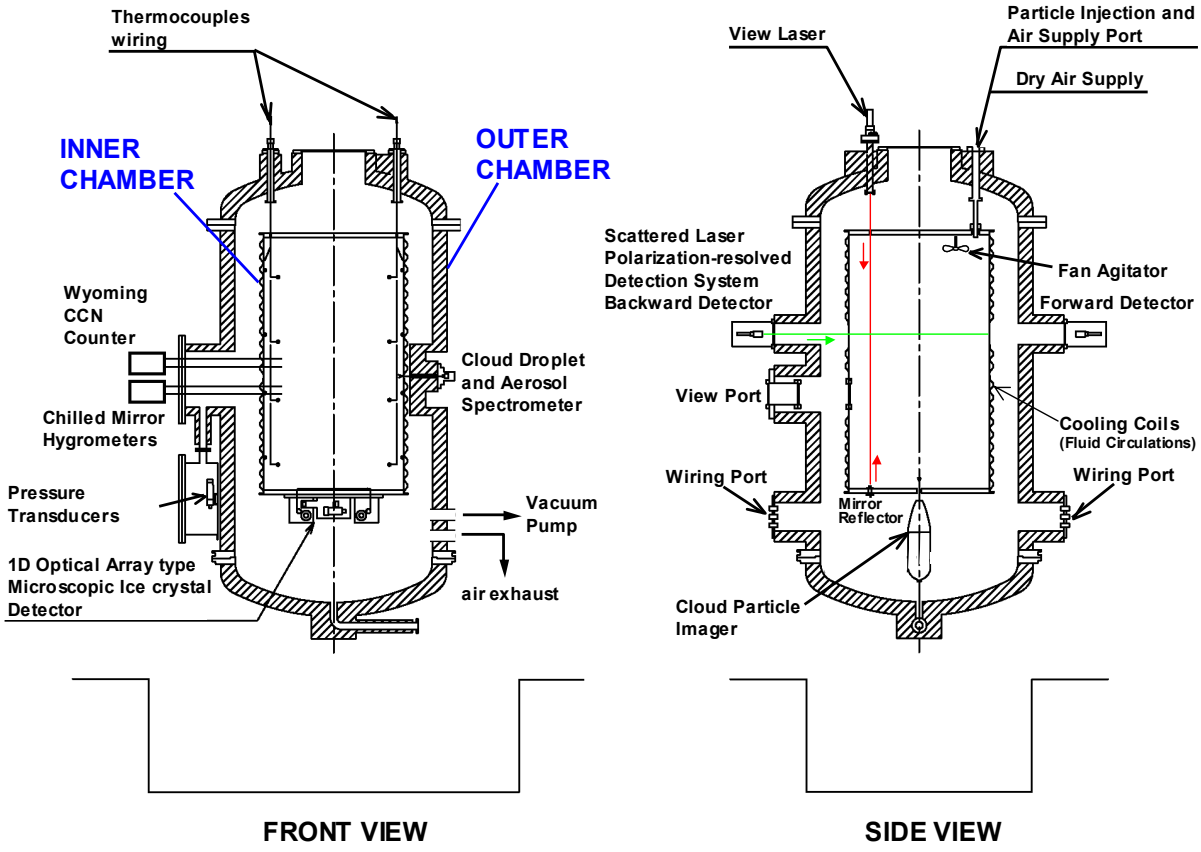

Fig. 1. Schematic diagrams of the MRI cloud simulation chamber.

fluid loop, which determines the cooling rate of the inner chamber, is regulated by a computer-controlled mixing valve. Its position depends on T_w and the temperature difference between T_w and the coolant reservoir temperature. The evacuation rate of air is regulated by a computer-controlled pressure-driven bypass valve. Its position depends on the chamber pressure and its lapse rate at the moment. During the ice formation experiments, the simulated ascents are designed to carry on dry adiabatic expansion until a temperature corresponding to the lifting condensation level (LCL) and moist adiabatic expansion thereafter. The initial condition of pressure, temperature, dewpoint temperature and ascent rate are necessary for calculating cooling/evacuation rate and LCL. The cooling/evacuation rate are controlled by data acquisition system (Model300, SEA) so as to produce adiabatic ascents covering a wide range of atmospheric conditions (30 to -100°C, 1000 to 30 hPa, 0 to 30 m/s). Accurate temperature and follow pressure controls are made by a combination of feed forward method and three-term PID control method. An example of programmed and actual ascent profiles is shown in Figure 3. In the succession of adiabatic ascent, the actual temperature and pressure are kept under the command profile within 0.5°C and 0.3hPa typically.

Experimental procedures are almost programmed, but during the pre-expansion period some manual procedures are currently required to prepare initial condition without delay. We expect to automate all procedures in the future.

Fig. 2. Photograph of the MRI cloud simulation chamber facility.

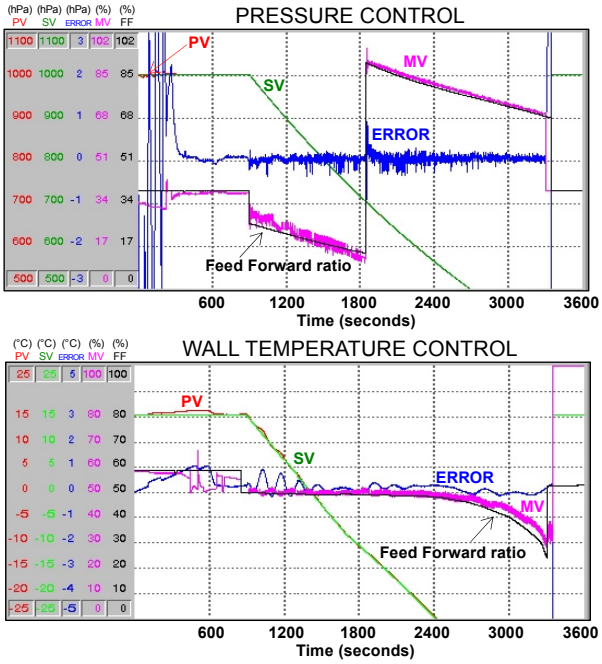

Fig. 3. Pressure (upper panel) and wall temperature (lower panel) versus time, displaying PV (actual), SV (program), ERROR (PV - SV), MV (valve position) and Feed Forward ratio through adiabatic ascent at 3 m/s.

4. DETECTION OF ICE FORMATION

The MRI chamber is equipped with various optical and electrical devices (Table 1) for sensing the cloud formation and measuring size distributions, shapes and sphericity of aerosol and cloud particles from 0.3 µm to 5 mm in size. Then, particles in the chamber can be characterized in several ways.

The onset of ice formation during an expansion is detected by measuring the depolarization of scattered laser beam (laser polarization-resolved detection system, SANKEI). Ice particles have a variety of shapes under the atmospheric conditions and the light scattering properties of particles are different between spherical and randomly orientated non-spherical particles. A laser beam (diode-pumped green crystal laser) operating at 532 nm is conducted into the chamber. Detection optics are mounted at scattering angles of 176° and 4°. The laser beam and the aperture of the detection optics overlap in the center of the chamber. The forward/backward scattered light intensity is split into the parallel and the perpendicular component to the polarization plane of the incoming laser and detected by a couple of two independent photomultipliers (R647, HAMAMATSU). The detection system is available for a precise determination of the formation and growth of cloud droplets and ice particles. Furthermore we would prefer to obtain quantitative information on the cloud properties.

Also, the onset of ice formation is simply identified by means of the view laser (HeNe 650nm), which was set on the top of the chamber and directed downward into the chamber. Scattering from the laser beam illuminates ice crystals, allowing the cloud to be seen through the viewing window in the middle of chamber. Cloud droplets scatter less brightness than Ice crystals.

The size distributions and the total concentrations of aerosol particles and cloud particles can be measured by drawing air at a known flow rate from the chamber volume to a optical particle counter, Cloud Aerosol Spectrometer (CAS, DMT), which is flange mounted directly on a side port of the chamber. The MRI chamber CAS system is adapted from the CAS unit used on the airborne Cloud Aerosol and Precipitation Spectrometer (CAPS). The instrument that has a pair of optical blocks (forward and backward scatter photo detector) detects particles by the amount of light they scatter in the forwards (4° to 12°) and the backwards direction (168° to 176°) when passing through a focused incident laser beam (680nm). The operating principle relies on the concept that the amount of light scattered by a particle is proportional to its size. The CAS has an additional function to record the forward and backscatter intensity for each particle on a Particle by Particle (PbP) basis. The PbP interface stores up to 204 sequential data at a time (sampling rate 10Hz). The liquid or solid phase can be determined, by making use of the fact that aspherical particles scatter significantly more light in backward than spherical particles, while near-forward scattered light is less affected. An on-board digital signal processor converts signal levels to particle sizing data and classifies individual particle into 30 size bins (forward 0.3 to 28.5 µm; backward 0.6 to 50 µm).

Cloud Condensation Nuclei (CCN) is measured with a static diffusion chamber (CCNC-100B, University of Wyoming) at 0.2, 0.4, 0.8, 1.2 and 2.0% supersaturation to produce the supersaturation spectra of cloud condensation nuclei. Sampling air is drawn from the experimental volume through a sampling tube to the detection chamber and periodically flushed. The CCNC is programmed to continuously cycle through a sequence of these supersaturations. A supersaturation is created by means of a temperature gradient between two plates having moist surfaces.

The flux of cloud droplets and ice crystals from the experimental volume is measured at the base of the chamber with a couple of devices. Two-dimensional images of cloud particles detected by Cloud Particle Imager probe (CPI, Lawson et al. 2001) yield detailed information on early ice formation; shapes and size distributions and concentrations of ice and cloud droplets. Particles are drawn into the instrument at a known flow rate, for CPI is used to operate as an airborne research instrument. A two-beam particle

Instrument	Measurement	Sampling Method	Status
View Laser	**Onset of Ice Formation** (Observing through Wiew Port)	**Scattering from Laser Illuminates Cloud particles** Laser Wavelength: 650nm (Red) Laser Power: 30mW	Operating
Laser sensor for Ice crystal Scattered Laser Polarization-resolved Detection System	**Onset of Ice Formation** **Formation and Growth of Cloud droplets** (Monitoring: Forward/Backward Scattered Light Intensity, Both Parallel and Perpendicular Component)	**A Couple of Two Photomultipliers (Forward/Backward)** A Laser Beam: Diode Pumped Green Crystal Laser Laser Wavelength: 532nm Scattering Angles: 4° (forward), 176° (backward)	Tentative Operating
Cloud droplet and Aerosol Spectrometer (**CAS**)	**Size distributions and Total Concentration of Aerosol and Cloud particles** Size Range: 0.3μm – 28.5 μm (forward) 0.6μm – 50 μm (backward) 30 Size Bins, selectable Sample Area: 1.1mm ×120μm Sample flow rate: ～1 L/min Concentration range: 0-10000 cm-3 Sampling Frequency: 0.1-10Hz	**Forward and Back Scatter sensors** Laser Wavelength: 680nm Light Collection Angle: 4° – 12° (forward) 168° – 176° (backward) **Particle by Particle (PbP)** A Sequential Forward and Backward scattering information: Maximum 204 Particles	Operating
Wyoming CCN Counter (**WyoCCNC**)	**Activity Spectra of Condensation Nuclei** (Periodically Repetition)	**Static thermal diffusion chamber** Supersaturation range: 0.2 – 2.0 % Laser diode: 670 nm	Operating
Cloud Particle Imager (**CPI**)	**Onset of Ice Formation, Shape and Size Distributions and Concentrations of Ice and Cloud droplets** Sample Area: 2.5mm ×2.5mm CCD resolution: 2.4 μm (1024×1024pixel) Sample flow rate: ～1 L/min Frame rate: Maximum 74 /sec Concentration range: 0-100 cm-3	**two-beam Particle Detection System (PDS)** PDS Laser Wavelength: 785nm PDS Laser Power: 40mW (CW) PDS beam size: 0.5mm × 2.5mm PDS Collection Angle: 2.5° – 8.2° **CCD camera with Imaging Laser** Imaging Laser Wavelength: 810nm Imaging Laser Power: 120W (Pulse)	Operating
Microscopic Ice crystal Detector (**1-D Optical Array Sensor**)	**Size Distributions and Number Concentrations of respective particle types** **Distinguish between Cloud droplets and Ice crystals** **Ice crystal habits** film speed: 1 to 50mm/s sensor resolution: 2.4 μm/pixel (2048 pixel)	**A Film Collection System** Collectiom surface: 16mm film (transparent) Free falling particle **1-D Array sensor**	Not Operating

Table 1. Summary of the instrument specifications for the MRI cloud chamber experiments.

detection system strobe a laser (785nm) to flash the instant a particle is in the imaging system object plane. A CCD camera with firing the imaging laser (810nm) records the frame (1024 × 1024 pixel) including the particle images. Each pixel in the array is 2.3μm, so it is available for measuring drops and ice crystals in the size range from 10μm to 2 mm. The image processing system analyzes the position of particles and their regions of interest in the frame for displaying and recording. The maximum frame rate is 74 per second, and since more than a hundred particles per frame can be processed, several thousands particles per second are detectable.

A microscopic ice crystal detector (produced by SANKEI) equipped with one-dimensional optical array sensor (line scan camera P2-21, DALSA) is another useful cloud particle measurement device. This system provides images with sufficient resolution (2.4 μm/pixel) to distinguish between cloud droplets and ice crystals, and can detect detail on ice crystal habits. The cloud particles fall onto the surface of 16mm transparent film which moves at moderate speeds (1 to 50mm/s) across the bottom of the inner chamber, through a small hole of the bottom plate coil, and go into the observation section of 1-D array sensor. As well as CPI, it is possible to evaluate the size distributions and the number concentrations for each particle types, considering a slight time lag (i.e., ice crystals must grow and settle down to the bottom of the chamber) in detecting ice crystals (e.g., DeMott and Rogers 1990). However it was not utilized for the experiment in this paper.

The data acquisition system, Model-300, gathers the data obtained from these instruments at 1 Hz or 10 Hz, except for CPI and the microscopic ice crystal detector which record the measured data to their own data acquisition systems.

5. RESULTS

Three experiments were performed to investigate ice formation processes under different sample air conditions. The intent is to appraise the performance of the MRI chamber to reproduce the cloud formation and ice initiation processes and sensibility of our instruments for cloud particle detection. Main parameters in the three experiments conducted in this preliminary study are listed in Table 2. The programmed initial pressure, temperature and adiabatic ascent rate were 1000hPa, 15°C, and 3m/s and were common to all three experiments. In the case of experiments #1 and #3, fresh air out of our cold environment simulator building was introduced into the chamber and was subsequently adjusted to acceptable T_{dew} by mixing with dry filtered air, Initial T_{dew} for #3 was by 6 K lower than that for #1. In the

experiment #2, smoke from mosquito-repellent incense was introduced into the chamber to simulate the aerosols from biomass burning.

Figure 4 shows the supersaturation spectrum of activated CCN in natural (outdoor) atmospheric air. The concentration of CCN during experiment #1 ranged from a few hundred to a thousand cm^{-3} at supersaturations between 0.2 and 2.0%.

In the experiment #1, adiabatic ascent (expansion) was conducted in the temperature range from 15°C to -40°C (as seen in Figure 5). Below -8.8°C (nearly the temperature at LCL), some of larger aerosol particles started to be activated (Figure 6), and grew up to cloud droplets (>10μm) before ice nucleation occurred (Figure 7). The conversion of cloud particles from the liquid phase to the ice phase was detected by CPI. The onset of Ice formation was at -18°C (t=1250) with coexisting cloud droplets. It also turned out that laser sensor and CAS were sensitive to the formation of both cloud droplet and ice crystal. Below -20°C, cloud droplets evaporated and size distributions from CAS (not shown) immediately came back to a pattern before cloud formation. After that (T_a<-23°C), ice crystals more than 10 particles/L were observed (Figure 8).

In the experiment #2, the onset of ice formation detected by CPI was at -23.5°C. High concentration of organic carbon particles formed numerous tiny cloud droplets, which may suppress ice initiation in rather warm temperature regions. Ice initiation became very active below -30°C.

In the experiment #3, the temperature of LCL was much lower than in experiment #1 so that cloud droplets formed were thinner than in experiment #1. The onset temperature of ice formation was -19.3°C and close to that in experiment #1. However the concentration of ice crystals was considerably less than in the experiment #1.

Experiment No.	#1	#2	#3
Programmed Initial Pressure (hPa)	1000.0	1000.0	1000.0
Programmed Initial Temperture (℃)	15.0	15.0	15.0
Programmed Adiabatic Ascent Rate (m/s)	3.0	3.0	3.0
Actual Initial Pressure (hPa)	999.9	999.9	999.9
Actual Initial Wall Temperture (℃)	15.2	15.0	15.0
Actual Initial Air Temperture (℃)	15.3	15.4	14.8
Initial Dewpoint Temperature (℃)	-4.7	-5.0	-10.9
Pressure at LCL (hPa)	742	736	674
Temperture at LCL (℃)	-8.6	-9.2	-15.8
Ascent Duration at LCL (sec)	804	823	1047
Sample Air injected into the Inner Chamber	Natural Air (Out-of-doors)	Natural Air with Smoke of Incense (Insecticide)	Natural Air (Out-of-doors)

Table 2. Parameters for 3 experiments. There are differences in sample air (#1:natural air; #2: polluted air; #3: same as #1, but lower T_{dew}).

The concentrations of ice crystal produced in the three experiments are shown in Figure 9. The maximum number concentrations were 23 / ℓ at -26°C (#1), 1600 / ℓ at -38°C (#2) and 10 / ℓ at -26°C (#3).

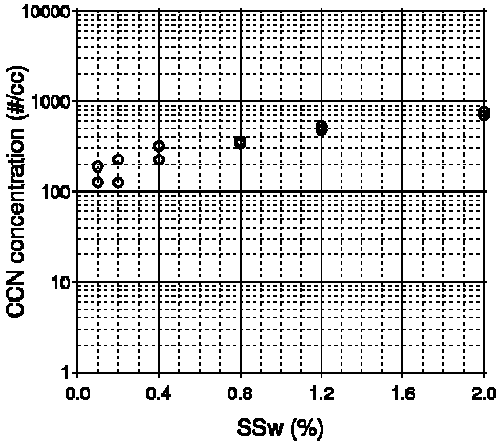

Fig. 4.Supersaturation spectrum of CCN in natural air prior to expansion (experiment #1).

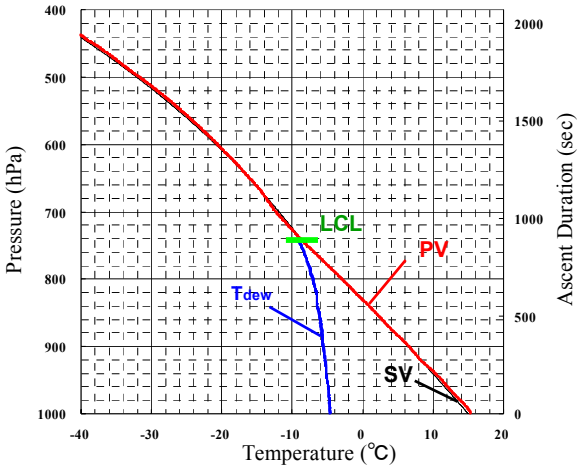

Fig. 5. An ascent profile (T_a versus Pressure) in experiment #1. T_{dew} until LCL is also shown.

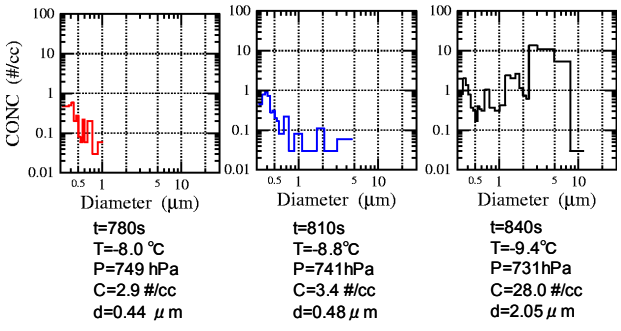

Fig. 6. Size distributions of aerosol and cloud particles measured by CAS (experiment #1). Particle growth abruptly occurs around LCL (t=804sec).

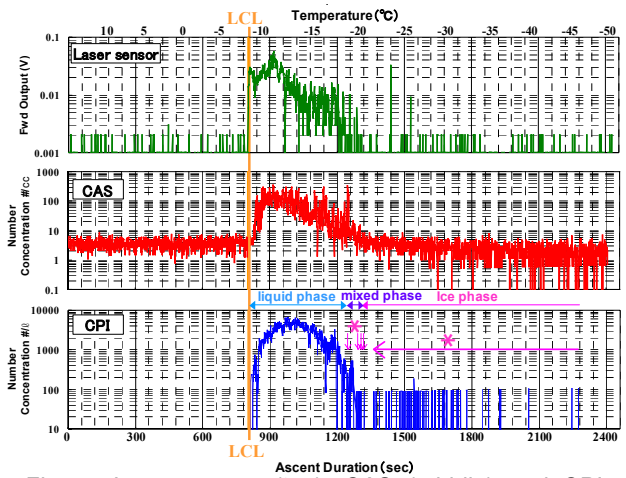

Fig. 7. Laser sensor (top), CAS (middle) and CPI (bottom) measurements during experiment #1. Timing of LCL is also shown. The arrows in bottom panel indicate the time when ice crystal images were taken by CPI.

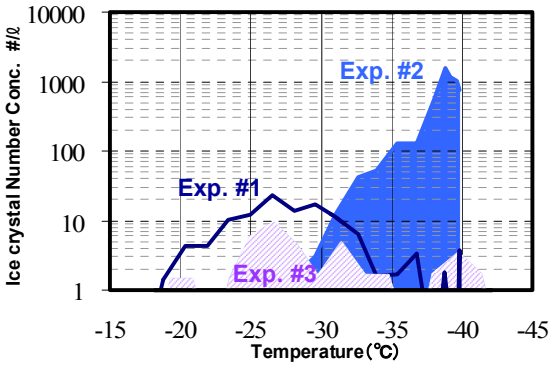

Fig. 9. Comparison of the number concentrations of ice crystals produced in 3 experiments. The concentration is averaged over one minute.

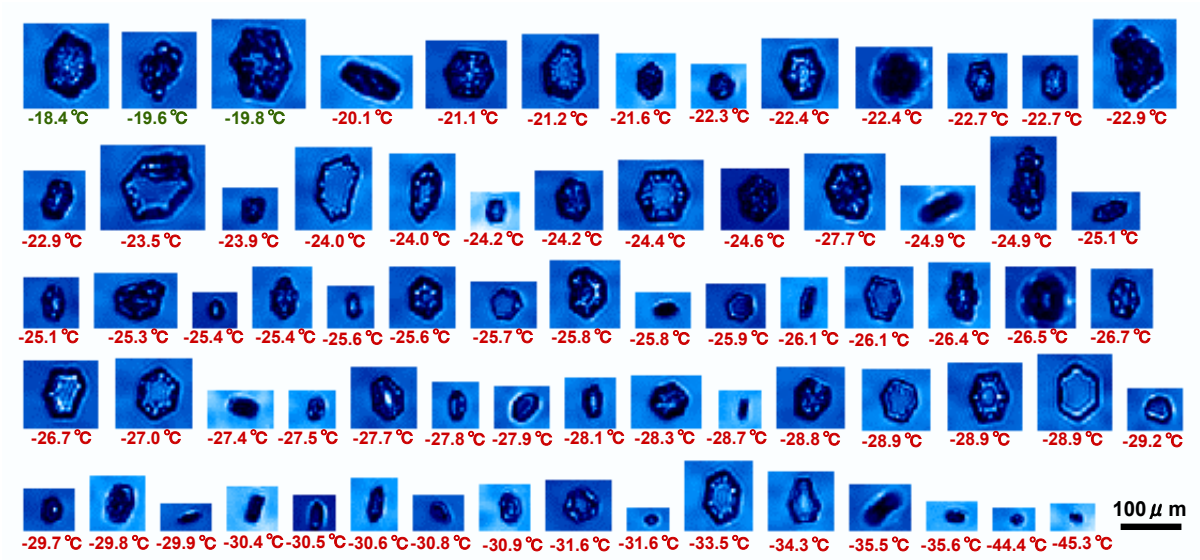

Fig. 8. Images of ice crystal measured by CPI in the MRI cloud chamber experiments (#1). Temperature at the time of particle detection is also shown

6. SUMMARY

MRI cloud simulation chamber began to run for preliminary experiments of ice formation. Various optical and electrical measurements can characterize aerosol and cloud particles in the chamber. A first set of experiments reported here demonstrated the usefulness of the chamber for cloud and ice formation experiments using specific aerosol particles as CCN and/or IN.

Data analysis showed that the concentrations of ice particles were approximately 20 / ℓ in -26°C and very high, exceeding 1000 / ℓ below -35°C. In the experiment, atmospheric air from out-of-doors was used as sample air.

More experiments are in progress to assess the dependence of the onset of ice nucleation, and the number concentrations of ice crystals on the air temperature and ascent rate. Results from the chamber experiments will be compared with in situ observations in near future.

7. *References*

DeMott, P.J., and D. C. Rogers, 1990: Freezing nucleation rates of dilute solution droplets measured between -30 and -40 C in laboratory simulations of natural cloud formation, *J. Atmos. Sci.*, **47**, 1056-1064.

Lawson, R. P., B.A. Baker, C.G. Schmitt, and T.L.

Jensen, 2001: An overview of microphysical properties of Arctic clouds observed in May and July 1998 during FIRE ACE. *J. Geophys. Res.*, **106** , D14 , 14989-15014.

Pruppacher, H. R. and J. D. Klett, 1997: Microphysics of clouds and precipitation. 2nd rev. and enl. ed., Kluwer Academic Publishers.